SPACE SCIENCES

Wave ripples formed in ancient, ice-free lakes in Gale crater, Mars

Claire A. Mondro[1]*, Christopher M. Fedo[2], John P. Grotzinger[1], Michael P. Lamb[1], Sanjeev Gupta[3], William E. Dietrich[4], Steven Banham[3], Catherine M. Weitz[5], Patrick Gasda[6], Lauren A. Edgar[7], David Rubin[8], Alexander B. Bryk[4], Edwin S. Kite[9], Gwénaël Caravaca[10], Juergen Schieber[11], Ashwin R. Vasavada[12]

Symmetrical wave ripples identified with NASA's Curiosity rover in ancient lake deposits at Gale crater provide a key paleoclimate constraint for early Mars: At the time of ripple formation, climate conditions must have supported ice-free liquid water on the surface of Mars. These features are the most definitive examples of wave ripples on another planet. The ripples occur in two stratigraphic intervals within the orbitally defined Layered Sulfate Unit: a thin but laterally extensive unit at the base of the Amapari member of the Mirador formation, and a sandstone lens within the Contigo member of the Mirador formation. In both locations, the ripples have an average wavelength of ~4.5 centimeters. Internal laminae and ripple morphology show an architecture common in wave-influenced environments where wind-generated surface gravity waves mobilize bottom sediment in oscillatory flows. Their presence suggests formation in a shallow-water (<2 meters) setting that was open to the atmosphere, which requires atmospheric conditions that allow stable surface water.

INTRODUCTION

Debate about the paleoclimate conditions on early Mars ranges from cold and wet scenarios, with abundant glaciogenic processes and limited standing water free of an ice cover [e.g., (1, 2)], to warm and wet scenarios, with abundant standing water free of ice [e.g., (3)]. While there is geomorphic evidence for surface water activity across Mars (3–8), the climate models lack consensus on the precise conditions, timing, and duration of surface water, specifically whether standing water would be stable in early Mars atmospheric conditions (1, 2, 9, 10). Detailed documentation of sedimentary structures preserved in ancient martian strata is an essential element for resolving this debate because they are capable of recording processes that preserve precise paleoenvironmental conditions, which are critical for constraining and validating climate models. Specifically, features such as wave ripples that are formed by the interaction of atmosphere, water, and sediment can be used to constrain both aqueous and atmospheric conditions (11).

Both Earth and Mars have (and had) a well-defined atmosphere, hydrosphere, cryosphere, and lithosphere. Processes within these systems generate currents of air, liquid water, and ice, which transport sediments from sites of weathering and erosion where they are formed to sites of deposition where they accumulate to create a record of sedimentary rocks (12). As on Earth, past surface processes on Mars, including within Gale crater—the site of exploration by NASA's Mars Science Laboratory rover Curiosity—are recorded as suites of sedimentary structures and lithologic textural parameters, which can be measured by orbiter and rover cameras and analytical instruments (13–18).

Here, we document the occurrence of symmetrical, shallow-water, wave-generated ripples at two different locations within the predominantly aeolian Mirador formation (19) within Gale crater, Mars. The sedimentary features documented here are the most definitive examples of wave oscillation ripples documented on another planet. Possible wave ripples have only documented once before in Gale crater (11), but in that case, other formation mechanisms could not be confidently ruled out. Wave ripples have so far have not been detected anywhere else on Mars. Symmetric wave ripples have specific environmental implications, as their formation requires sediment transport and deposition by oscillatory currents acting on a shallow lake bottom as a result of wind-generated gravity waves on the lake surface. In the case of Mars, wave-ripple formation requires a climate with sufficiently higher atmospheric pressure, warmth, and humidity than at present to sustain surficial bodies of liquid water absent of an ice cover. To reconcile the geomorphic evidence for lakes with early Mars climate models, previous studies have suggested that water bodies on Mars would have been ice covered (20–22). Observations of wave ripples disprove this long-standing hypothesis and provide a key geologic constraint on the depositional environment and associated climate models.

Geologic and stratigraphic context

Since arriving at the Bradbury landing site in Gale crater in 2012, the Curiosity rover has ascended the northern slopes of Aeolis Mons (informally known as Mount Sharp), climbing more than 800 m of elevation along a traverse more than 32 km in length. The rocks that now comprise the ~5-km high sedimentary mound within Gale crater were deposited during Hesperian time, ~3.0 to 3.7 billion years ago (23). The stratigraphic succession has been divided into group-level packages (Mount Sharp and Siccar Point), which, in turn, are

[1]Division of Geological and Planetary Sciences, California Institute of Technology, Pasadena, CA 91125, USA. [2]Department of Earth and Planetary Sciences, University of Tennessee, Knoxville, TN 37996, USA. [3]Department of Earth Science and Engineering, Imperial College London, London, UK. [4]Earth and Planetary Science, University of California, Berkeley, Berkeley, CA 94709, USA. [5]Planetary Science Institute, Tucson, AZ 85719, USA. [6]Los Alamos National Laboratory, Los Alamos, NM 87545, USA. [7]U.S. Geological Survey Astrogeology Science Center, Flagstaff, AZ 86001, USA. [8]Department of Earth and Planetary Sciences, University of California, Santa Cruz, Santa Cruz, CA 95064, USA. [9]Department of the Geophysical Sciences, University of Chicago, Chicago, IL 60637, USA. [10]Institut de Recherche en Astrophysique et Planétologie, Université de Toulouse CNRS, CNES, Toulouse, France. [11]Department of Earth and Atmospheric Sciences, Indiana University, Bloomington, IN 47405, USA. [12]Jet Propulsion Laboratory, California Institute of Technology, Pasadena, CA 91109, USA.

*Corresponding author. Email: cmondro@caltech.edu

subdivided into mappable formation- and local member-level sub-units (Fig. 1). On the basis of the observation that Mount Sharp strata are horizontal or close to horizontal in attitude (14, 24–26), we use elevation as a proxy for stratigraphic thickness.

Along Curiosity's traverse up-section through the Mount Sharp group, the stratigraphy records an overall transition from more aqueous to more aeolian depositional environments. The Murray formation is dominantly composed of laminated mudstone representative of having been deposited in lacustrine and lacustrine-margin paleoenvironments (14, 17, 24, 25, 27–29). Several members within the Murray formation consist of finely laminated mudstones with few obvious stratigraphic discontinuities, which have been interpreted to represent long episodes of lake deposition with standing water (14, 15, 17). The Carolyn Shoemaker formation (Fig. 1D) records an overall shallowing-up sequence of interbedded lacustrine mudstones and marginal and fluvial sandstones (19, 30, 31).

The overlying Mirador formation marks a transition into predominantly aeolian depositional environments (Fig. 1D). Collectively, the Dunnideer, Port Logan, and Contigo members encompass 160 m of aeolian sand containing decimeter- to multimeter-scale trough cross-stratification (19). The Prow outcrop is one of the multiple lenticular deposits interstratified within the Contigo aeolian sandstones [(32); fig. S1]. The Catrimani member is composed of thin, planar, aeolian laminae (19), directly overlain by the Amapari Marker Band (AMB). The AMB is identifiable in orbital data as a dark, erosionally resistant bench (Fig. 1C) that can be traced nearly continuously along the northwest side of Mount Sharp (33, 34).

RESULTS
AMB outcrop

Curiosity first approached the AMB at the Amapari location (Fig. 1C) along the west side of Marker Band Valley (MBV). Alternating centimeter-scale resistant and recessive beds make up the lower unit of the AMB, containing structures interpreted as symmetric ripples (Fig. 2). The AMB, including the ripple unit, outcrops continuously around MBV. At the Amapari location, the ripple unit is 15 cm thick and contains five resistant rippled beds. The top of the uppermost ripple bed is a sharp contact with an overlying thickly laminated unit (Fig. 2C) that transitions into the thin, planar, aeolian laminae of the Chenapau member.

The ripples within the AMB resistant beds are composed of parallel millimeter-scale laminae that can be traced continuously through the ripple troughs and crests (Fig. 2A and fig. S2). Individual resistant beds are 1 to 2 cm thick. Internal laminae within the recessive beds (where visible) appear to uniformly drape the rounded ripple crests and define upward building of the ripples (fig. S3). The ripple crests in successive resistant beds are aligned near-vertically with no observed truncation of crests or laminae (Fig. 2A), indicating ripples formed by vertical accretion with little translation during higher sediment fallout. The rapid sedimentation during ripple formation and the darker tone of the AMB outcrop relative to the underlying stratigraphy suggest that the ripple layers are not formed from locally reworked lakebed sediments. The sediment was most likely sourced from further away, either as wind-blown sediment or in surface runoff from a location beyond the Amapari outcrop location.

At the Amapari location within the AMB, the ripples have an average wavelength (λ) of 4.5 cm, with a range of 3.83 to 5.32 cm (table S1). The symmetry index ranges from 0.73 to 1.20 (mean = 0.96), indicating that the ripples are symmetrical, consistent with ripples formed from oscillatory currents under surface gravity waves known as wave ripples. The average ripple height (h) is 0.66 cm and the average aspect ratio (h/λ) of the ripples is 0.13, which is consistent with orbital wave ripples (35). The grain size of the ripple beds is fine sand or smaller, as it is not detectable in Mars Hand Lens Imager (MAHLI) images (36). Linear ripple crests with occasional tuning-fork bifurcation, also
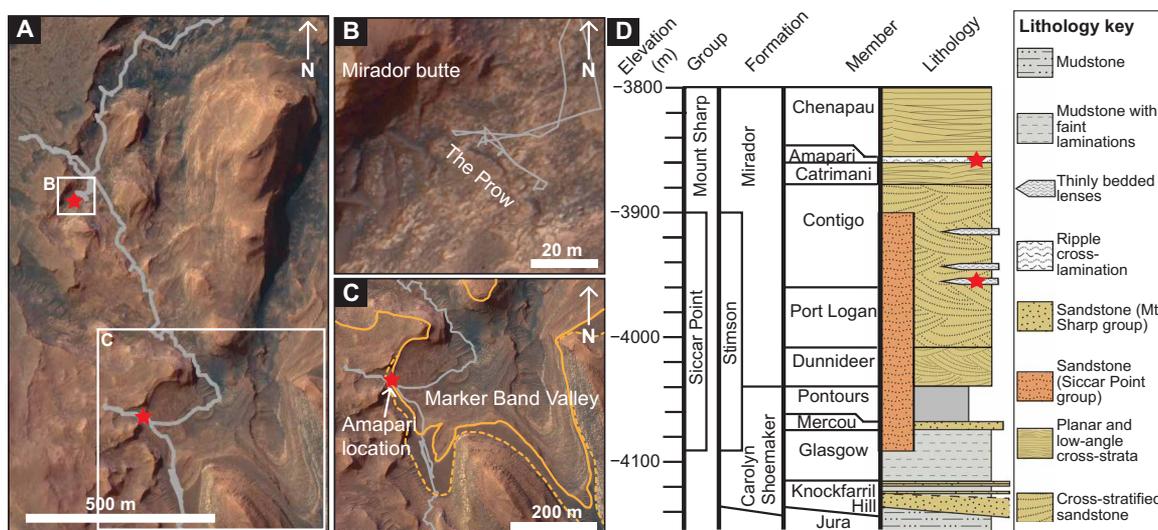

Fig. 1. Location of the Amapari Marker Band and Prow outcrops. Along the Curiosity traverse [(**A**), gray line] through the Mirador formation, the rover observed symmetric ripple marks within the Prow outcrop near the base of Mirador butte at elevation −3950 m (**B**) and the Amapari Marker Band (AMB) outcrop along the west side of Marker Band Valley (MBV) at elevation −3860 m (**C**). Red stars indicate the locations of the ripple-containing outcrops within the stratigraphic column (**D**) along the MSL traverse (A). The Prow is one of the multiple lenticular outcrops within the Contigo member. The AMB outcrops are nearly continuously around MBV [(C): solid orange line], often forming flat, erosionally resistant benches (inner edge traced in dashed orange line). The basemap used in (A) to (C) is a Mars Reconnaissance Orbiter HiRISE mosaic generated by Calef *et al.* (61, 62) and accessed through the NASA Planetary Data System.
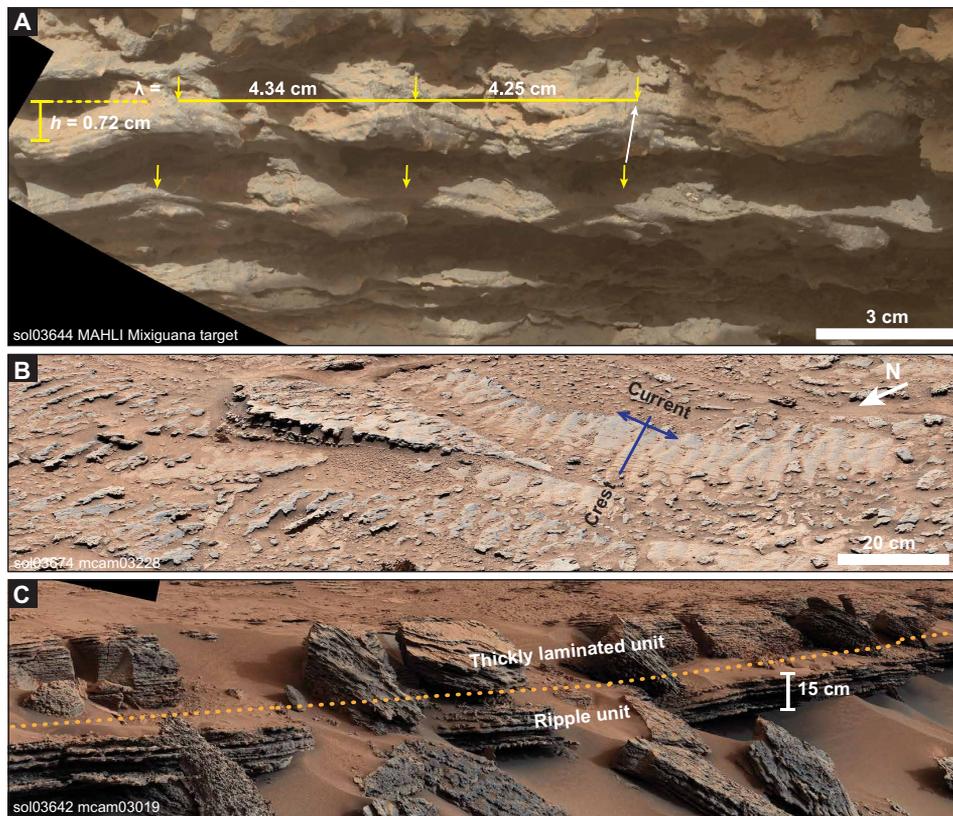
Fig. 2. Symmetric ripple marks in the AMB outcrop. Symmetric ripple marks (**A**) are observed within the AMB outcrop. Ripple crests are identified with yellow arrows (A) and are aligned near-vertical (white arrow) in successive ripple layers. Internal laminae can be traced continuously through the ripple troughs. In plan view (**B**), the ripple crests are linear with occasional tuning-fork bifurcation, oriented consistently NW/SE. The AMB ripple unit is laterally extensive, of consistent thickness, and is conformably overlain by a unit of planar laminae [(**C**): contact is covered here—dotted line is inferred contact]. The AMB ripple unit at the Amapari location is ~15 cm thick and is composed of five resistant beds containing symmetric ripple marks. Image credit: NASA/JPL-Caltech/MSSS.

consistent with oscillation ripples (*37*), are seen in planview along the top of the AMB bench at the Amapari location (Fig. 2B), oriented consistently southeast-northwest (table S1 and texts S1 and S2).

Prow outcrop
The Prow outcrop is an ~18-m-long and up to 0.7-m-thick lenticular outcrop (Fig. 3A) located near the base of Mirador butte in the Contigo member [(*32*); Fig. 1B and fig. S1]. At the base of the Prow is a ~40-cm-thick section of decimeter-scale cross-bedding indicating unidirectional flow to the east (Fig. 3C). This unit is overlain by a ~30-cm interval of flaser bedding where sand ripples and wavy beds are interbedded with fine-grained sediment drapes (Fig. 3, B and E). Near the top of the flaser bedded interval, symmetric ripples appear in single layers and amalgamated ripple stacks (Fig. 3, C and D). The amount of sedimentation and the stratigraphic pattern through the outcrop suggest that the Prow was not formed of predominantly reworked sediment from the stratigraphy directly underlying the outcrop. The distance to the sediment source is unclear from the data examined here and the sediment could have been transported via either wind or water from beyond the water body.

Ripple crests and troughs are both variably preserved throughout the rippled layer in a complex and interwoven cross-stratification pattern (*37*). The ripples are composed of fine to medium sand (median grain diameter, $D_{50} = 389$ μm) and the draping sediment is

very fine sand or finer (Fig. 3E), below the limit of resolution of MAHLI images (*36*).

Within the Prow the symmetric ripples have an average wavelength of 4.6 cm, with a range of 3.48 to 5.86 cm (table S2 and text S2). The symmetry index ranges from 0.78 to 1.16 (mean = 1.00), indicating that the ripples are symmetrical, consistent with ripples. The average ripple height is 0.35 cm and the average aspect ratio (h/λ) of the ripples is 0.074. Ripple crests are oriented approximately NNE/SSW (table S2), perpendicular to the outcrop face (Fig. 3B).

Wave-generated origin
Distinguishing between current and wave-influenced ripples depends on the wavelength and symmetry of the ripples. On Earth, current ripples in sand (i.e., from unidirectional flow) generally form at wavelengths of 8 cm and larger and are expected to be slightly larger under reduced gravity on Mars (*38*). Wave ripples, in contrast, can form at smaller wavelengths. The ripples in both the AMB and the Prow have wavelengths <6 cm (mean = 4.5 and 4.6 cm, respectively), which is smaller than current ripples are expected to form. Wave ripples have a symmetry index of <1.5, while current ripples have a symmetry index of 3.0 or greater (*39*). The symmetry indices of both the AMB and Prow ripples are consistent with symmetric wave ripples. On the basis of the wavelength and symmetry measurements, our conclusion is that both sets of ripples are wave influenced.
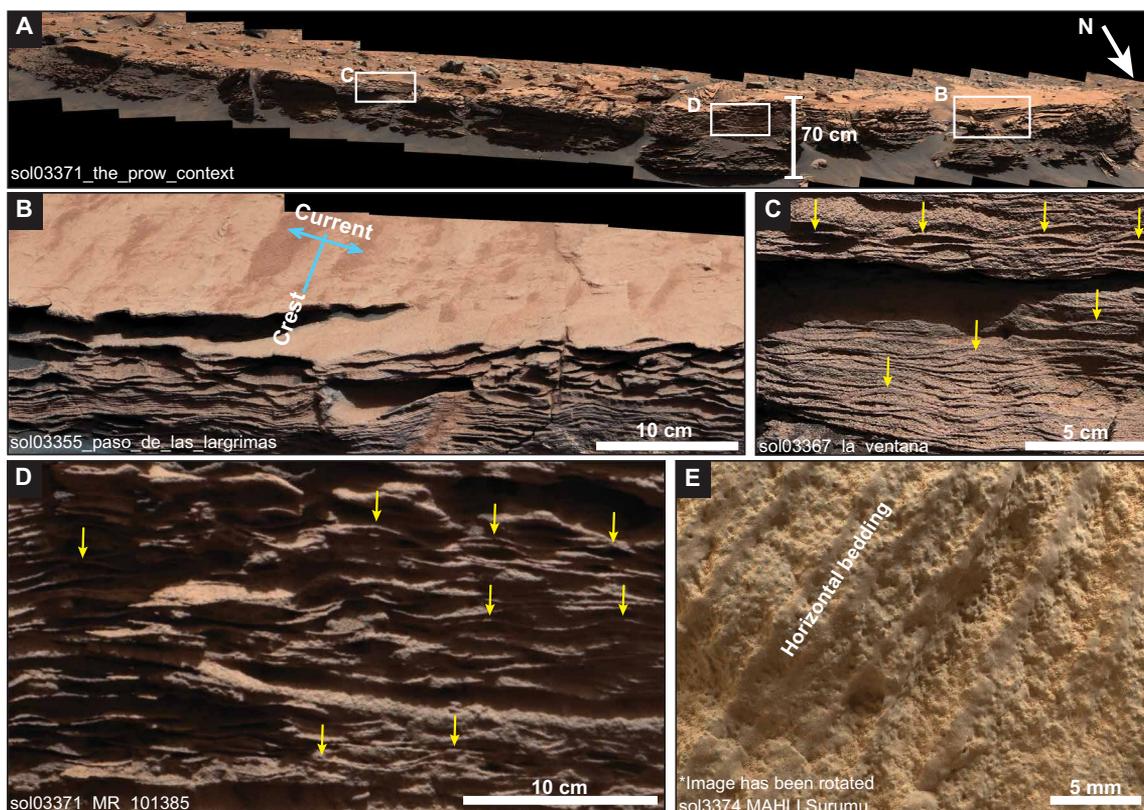
Fig. 3. Symmetric ripple marks in the Prow outcrop. The Prow is an 18-m-long, lenticular outcrop (**A**) composed of a lower unit of unidirectional cross-strata and an upper unit of flaser bedding (**B**) containing symmetric ripple marks [(**C** and **D**): ripple crests indicated by yellow arrows]. The vertical accumulation of ripple marks within the flaser bedding creates a complex patter of interwoven cross-lamination [as in (*34*), figure 8, ex. 9], preserving both symmetric ripple troughs and crests at various locations. High-resolution imaging by the MAHLI taken at 1 cm standoff from the outcrop (**E**) shows observable sand grains making up the ripple layers, draped by fine-grained material with no observable grains (grain size <180 μm, below the MAHLI limit of resolution). See fig. S4 for location context for (E). Image credit: NASA/JPL-Caltech/MSSS.

Within wave-influenced ripples, there exist orbital and anorbital wave ripples, and combined flow ripples. Orbital ripples have wavelengths that scale linearly with wave orbital diameter (*35*), whereas anorbital ripples do not. Combined flow ripples develop in the combined presence of waves and a unidirectional current. Two criteria are primarily used to differentiate between orbital and anorbital wave ripples. First, the aspect ratio (h/λ) of orbital ripples is typically >0.1 while the aspect ratio of anorbital ripples is typically <0.1. However, aspect ratios of 0.7 to 0.11 often fall into a transitional or suborbital regime (*35*). Second, the wavelength–to–grain size ratio (λ/D_{50}) of anorbital wave ripples consistently falls within the range of 400 to 600, while the λ/D_{50} of orbital ripples can be any value within the range of 100 to 2000, inclusive of 400 to 600 (*35*). The mean aspect ratio of the AMB ripples (0.13) is consistent with orbital ripples. The estimated λ/D_{50} of the AMB (250 to 750; see text S2) is nondiagnostic and could correspond to either anorbital or orbital ripples. The laminae patterns within the AMB ripples (Fig. 2) are indicative of symmetric orbital ripples.

The Prow ripples are less definitive. The aspect ratio (mean = 0.074) is inconsistent with orbital ripples and falls within the transition zone that may indicate suborbital or anorbital. However, the λ/D_{50} of 118 is inconsistent with anorbital ripples. A possible explanation is that the Prow ripples were formed in a combined flow environment.

Combined flow, where wave oscillation is superimposed on a unidirectional current, would make sense with the stratigraphic pattern of the outcrop. Near the base of the outcrop, the cross-strata are consistent with a predominantly unidirectional current before the onset of ripple formation. The symmetry index and aspect ratio of combined flow ripples fall within the same ranges as for symmetric wave ripples (*40*). The rounded crests of the Prow ripples are consistent with cross-strata patterns of combined flow (*40*). Cross-strata within individual ripples are rarely detectable at the image resolution available but one ripple example shows a potential example of laterally accreting laminae within a symmetric ripple (fig. S5). On the basis of ripple morphology and grain size characteristics, we conclude that the Prow ripples are wave influenced, and likely either suborbital or combined-flow ripples.

It is possible for small symmetric ripples to form in other environments (aeolian or fluvial) but the diagnostic ripple morphology and associated sedimentary features in such environments are inconsistent with the AMB and Prow ripples. Most notably, the wavelengths of the AMB and Prow ripples are inconsistent with current ripples, which exclusively form as longer wavelengths (*38*). The most likely non-lacustrine ripple-forming environment would be aeolian, given the surrounding aeolian strata through the Mirador formation. However, in this setting, which is dominated by exposure and deflation

with lag concentration of coarser particles (*41*) and abundant asymmetric wind ripple lamination, it is rare to find symmetric ripples or preserved ripple crests, and sedimentation processes preclude the formation of high-angle climbing ripples. Aeolian sand sheets along the margins of dune fields where the local conditions prevent formation of large dunes (*42, 43*) can contain flat laminae and wind ripples, but ripple wavelengths would still be larger than those observed in the AMB and Prow. In addition, the AMB and Prow outcrops represent distinct aberrations from the surrounding aeolian strata in tone and lamination patterns. Symmetric appearing ripples have been observed in fluvial settings on Earth and Mars (*15, 44–46*) where vertically accreting climbing ripples appear within a fluvial bar. However, the scale of ripple bedforms in these settings is substantially larger than the symmetric ripples of the AMB and Prow, which are smaller than the typical size of current ripples in sand (*38*).

The most plausible environmental interpretation for the ripples observed in the AMB and Prow outcrops is formation via the episodic impingement of surface gravity waves onto lake-floor sediment where resultant oscillatory shear stresses mobilized sediment in oscillatory flows to generate wave ripples (*47*). Given that our preferred interpretation of the ripples is that they are wave generated, we have modeled potential conditions for making these structures under wind-driven oscillatory flow conditions on Mars.

Modeling constraints

Results of the wave-ripple modeling (see text S3) illustrate that the AMB ripples could form on Mars under the assumed modeled conditions. The atmospheric density at the time of deposition is unknown, so we used values for modern Mars (0.02 kg m^{-3}) and modern Earth (1.2 kg m^{-3}) as illustrative bounds. Under modern Mars conditions, a wind speed of 25 to 100 m/s is needed to form the AMB ripples assuming a fetch of 500 m (Fig. 4). Although this speed is greater than has been directly measured on Mars by rovers (*48*), numerical models indicate that such wind speeds likely drove sand transport and dune development (*4*). In a denser atmosphere, required wind speeds are lower to produce the same waves (Fig. 4 and text S3), such that AMB ripples might have formed under more modest winds in a thicker early Mars atmosphere.

Ripples this small require shallow water depths (<2 m) under a range of wind speed and fetch conditions (fig. S6). If the fetch is kilometers or larger, predicted wind speeds are smaller, and the water depth must be <~1.5 m to limit wave growth; otherwise, most wind conditions would produce ripples larger than those observed (fig. S6A). Fetch smaller than 500 m requires larger wind speeds to move sand, and for fetch <~100 m, pure oscillatory ripples of this size do not form because the waves would break (fig. S6B).

Thus, the ripple formation conditions and water depths we estimated for the AMB are consistent with these structures as having formed by oscillatory flows under surface gravity waves in a shallow water body (<2 m).

DISCUSSION
Ripple depositional environment

The ripple unit of the AMB is more laterally extensive than the Prow, outcropping nearly continuously around the 500-m-wide MBV. The lateral extent is consistent with the model results, which indicate that the wave ripples can form in a range of fetch lengths, at least 200 to 500 m across. The ripple wavelengths indicate that the AMB
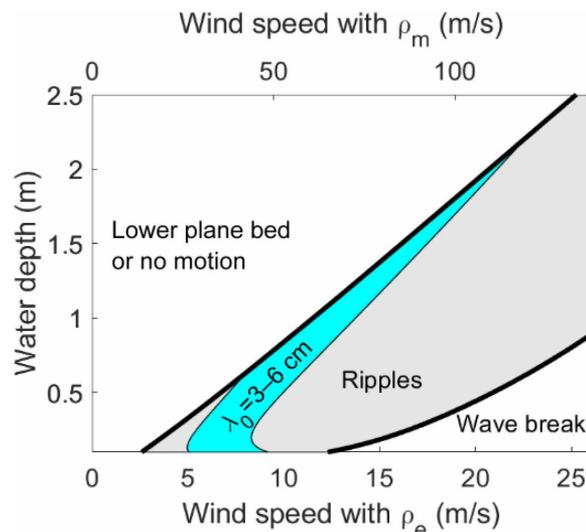

Fig. 4. Modeled water depth and wind speed of AMB ripples. Conditions to produce orbital wave ripples with 3 to 6 cm wavelength (blue shaded zone) with a fetch of 500 m and for 100 μm of sand (text S3). Wind speeds are calculated for modern Earth (ρ_e = 1.2 kg/m^3) and Mars (ρ_m = 0.02 kg/m^3) atmospheric densities. Larger depths under similar wind speeds would produce boundary shear stresses below the requirement to form ripples according to Myrow *et al.* (*54*), producing lower plane bed or no sediment motion. Faster wind speeds would produce larger ripples (gray shaded zone) or breaking waves that do not produce orbital ripples. Changing the fetch from 200 to 5000 m results in small changes to the predicted wind speeds to produce the observed ripples, and requires similarly small water depths (fig. S6).

ripples, distributed around MBV, formed in a water body less than 2 m deep and approximately 500 m wide. The successive beds of ripples indicate frequent wind activity throughout 15+ cm of sediment deposition. The occurrence of this interval between the Catrimani and Chenapau members represents an accumulation of ice-free surface water, 110 m stratigraphically above and larger in area than the Prow inter-dune lakes, amidst a predominantly aeolian regime.

Even without a precise water depth model, the Prow ripples, of similar wavelength to the AMB ripples and with morphology consistent with suborbital or combined flow ripples, could have formed in relatively shallow water similar to the modeled AMB environment. Within the Prow, the lamination patterns suggest that lateral sediment transport along the base of the lacustrine environment transitions to rapid sedimentation during wind activity, interspersed by periods of calm that allow fine-grained sediment drapes to settle out of suspension.

Implications for martian paleoclimate

Geomorphic features, such as fluvial drainage networks and fan deposits that infill craters, indicate that Mars experienced an active rain- or snowfall-based hydrologic cycle at the surface during the Noachian and Early Hesperian (*3–8*). While geologic evidence points to water-formed features on the surface of early Mars, current climate modeling is inconclusive on specifically the stability of persistent, ice-free, standing water at the surface (*1, 2, 9, 10*). Previous work has repeatedly proposed that standing water on the surface could have been ice covered (*20–22*), which would provide an explanation for both the geomorphic evidence and the conditions suggested by the

climate models. Wave ripples are uniquely diagnostic of standing water that is free of ice, as other lacustrine sedimentary features can form from various processes or in a wider range of conditions. The wind-generated wave ripples presented here contribute geologic evidence for two separate instances where an accumulation of surface liquid water up to 2 m deep was open to the atmosphere and experienced wind-generated wave activity throughout the deposition of tens of centimeters of sediment. The precise formation conditions of the wave ripples provide critical constraints on possible pressure and temperature conditions of Mars atmosphere to allow for an ice-free lake surface at the time of formation, which will inform or validate ongoing climate modeling.

These surface lakes within the Mirador formation are consistent with an active Hesperian hydrologic cycle that involved stable liquid water free of an ice cover. Climate modeling calculations (*2*) suggest that open water lakes in the Hesperian in Gale were unlikely and proposed ice-covered lakes supported by glacial melt water despite the lack of evidence of glacial deposits in the stratigraphy of Gale (*24*). One orbiter-based study concluded that large-scale geomorphic features within Gale may have formed in a glacial/periglacial setting (*1*), but in situ rover-based studies have not provided evidence for glacial processes or landforms. Rather, rover-based studies of bedrock features at Gale show that buttes and ridges are remnants of aeolian abrasion of older strata (*26*, *49*, *50*). It is also noteworthy that sequences of sedimentary rocks at Meridiani Planum and Gusev crater, also of Early Hesperian age, do not preserve evidence of past glaciation in the early history of Mars (*15*, *51*–*53*). Thus, whereas glacial processes may have influenced landscapes in the later history of Mars, the earlier history of Mars, preserved in its stratigraphic record, bears no evidence for ice-controlled deposition as observed by multiple rovers deployed in diverse locations.

The formation of the centimeter-scale wave ripples described here requires the activity of oscillatory flows and the transmission of surface wave energy to a shallow lake bed. The sedimentologic evidence for ripples created by wind-water interaction leads us to conclude that the lakes in which the ripples formed were free of ice and open to the atmosphere. Our modeling indicates that, under a range of relevant parameters, the wave-generated ripples could form at the observed scale. The occurrence of the wave ripples within Gale crater stratigraphy suggests that shallow lakes formed multiple times at successive stratigraphic intervals. Collectively, the ripples preserved in the Mirador formation provide strong evidence for a climate warm and humid enough to permit recurring open-water lakes during this 110-m aeolian depositional interval in Gale crater.

MATERIALS AND METHODS
We performed visual assessment of morphology and sedimentary features within both the AMB and Prow outcrops using Mast camera (Mastcam) image mosaics collected with the Mars Curiosity rover. Curiosity imaged the marker band outcrop at the Amapari location along the west side of MBV (Fig. 1). Up-close, orthogonal views of the centimeter-scale ripples were collected at one location and distance imaging was collected to the north and south along the outcrop from the same location. Curiosity then crossed over the top of the AMB, collecting detailed imaging of the top of the ripple layer. Ripple morphology measurements were primarily performed using MAHLI and Chemistry & Camera long-distance Remote Micro Imager image data (text S1). Morphology measurements, including

mean and range of each parameter for each ripple population, are included in tables S1 and S2.

Using the wavelength measurements from the AMB ripple marks, we conducted wave-ripple modeling to determine whether the observed orbital, symmetric ripples could form in a range of early Mars–appropriate conditions (Fig. 4). Because the Prow wave-ripple morphology is inconclusive as to orbital versus anorbital, we did not perform separate wave modeling for the Prow environment. If the Prow ripples are suborbital or combined flow, the environment could be similar to that modeled for the AMB, given the similarity in wavelengths. If the Prow ripples are anorbital, that could allow for deeper water or larger waves than the AMB environment (*54*).

We calculated the wave heights and wave periods for a given wind speed using a wave forecasting model (*55*), which we adopted for Mars gravity and atmospheric density (see texts S3 and S4). Following Lamb *et al.* (*56*), we combined the outputs from the wave model and Airy wave theory to calculate the water depths and wind speeds required to produce the near-bed orbital diameters (AMB: $d_o = 0.069$ m) that are consistent with the observed orbital ripple wavelengths (where $\lambda = 0.65 d_o$ for orbital ripples; see text S3). In addition to producing the necessary orbital diameters, wave oscillations must have been strong enough to have transported sediment to produce stable ripples. Assuming a median grain size of 100 μm (very fine sand), we used bedform stability constraints (*57*) to find the water depth and wind-speed combinations where ripples are stable (Fig. 4).

Supplementary Materials
This PDF file includes:
Supplementary Text S1 to S4
Figs. S1 to S6
Tables S1 and S2
References

REFERENCES AND NOTES
1. A. G. Fairén, C. R. Stokes, N. S. Davies, D. Schulze-Makuch, J. A. P. Rodríguez, A. F. Davila, E. R. Uceda, J. M. Dohm, V. R. Baker, S. M. Clifford, C. P. McKay, S. W. Squyres, A cold hydrological system in Gale crater, Mars. *Planet. Space Sci.* **93-94**, 101–118 (2014).
2. A. M. Kling, R. M. Haberle, C. P. McKay, T. F. Bristow, F. Rivera-Hernandez, Subsistence of ice-covered lakes during the Hesperian at Gale crater, Mars. *Icarus* **338**, 113495 (2020).
3. R. M. Ramirez, R. A. Craddock, The geological and climatological case for a warmer and wetter early Mars. *Nat. Geosci.* **11**, 230–237 (2018).
4. N. G. Barlow, *Mars: An Introduction to Its Interior, Surface and Atmosphere* (Cambridge Univ. Press, 2009).
5. A. D. Howard, J. M. Moore, R. P. Irwin III, An intense terminal epoch of widespread fluvial activity on early Mars: 1. Valley network incision and associated deposits. *J. Geophys. Res. Planets* **110**, E12S14 (2005).
6. M. C. Malin, K. S. Edgett, Sedimentary rocks of early Mars. *Science* **290**, 1927–1937 (2000).
7. N. Mangold, C. Quantin, V. Ansan, C. Delacourt, P. Allemand, Evidence for precipitation on Mars from dendritic valleys in the Valles Marineris area. *Science* **305**, 78–81 (2004).
8. R. D. Wordsworth, The climate of early Mars. *Annu. Rev. Earth Planet. Sci.* **44**, 381–408 (2016).
9. E. S. Kite, L. J. Steele, M. A. Mischna, M. I. Richardson, Warm early Mars surface enabled by high-altitude water ice clouds. *Proc. Natl. Acad. Sci. U.S.A.* **118**, e2101959118 (2021).
10. R. Wordsworth, A. H. Knoll, J. Hurowitz, M. Baum, B. L. Ehlmann, J. W. Head, K. Steakley, A coupled model of episodic warming, oxidation and geochemical transitions on early Mars. *Nat. Geosci.* **14**, 127–132 (2021).
11. D. M. Rubin, M. A. G. Lapôtre, A. W. Stevens, M. P. Lamb, C. M. Fedo, J. P. Grotzinger, S. Gupta, K. M. Stack, A. R. Vasavada, S. G. Banham, A. B. Bryk, G. Caravaca, J. R. Christian, L. A. Edgar, M. C. Malin, Ancient winds, waves, and atmosphere in Gale crater, Mars, inferred from sedimentary structures and wave modeling. *J. Geophys. Res. Planets* **127**, e2021JE007162 (2022).
12. J. P. Grotzinger, A. G. Hayes, M. P. Lamb, S. M. McLennan, Sedimentary processes on earth, Mars, titan, and Venus, in *Comparative Climatology of Terrestrial Planets* (University of Arizona Press, 2013), pp. 439–472.

13. S. G. Banham, S. Gupta, D. M. Rubin, J. A. Watkins, D. Y. Sumner, K. S. Edgett, J. P. Grotzinger, K. W. Lewis, L. A. Edgar, K. M. Stack-Morgan, R. Barnes, J. F. Bell, M. D. Day, R. C. Ewing, M. G. A. Lapotre, N. T. Stein, F. Rivera-Hernandez, A. R. Vasavada, Ancient Martian aeolian processes and palaeomorphology reconstructed from the Stimson formation on the lower slope of Aeolis Mons, Gale crater, Mars. *Sedimentology* **65**, 993–1042 (2018).

14. L. A. Edgar, C. M. Fedo, S. Gupta, S. G. Banham, A. A. Fraeman, J. P. Grotzinger, K. M. Stack, N. T. Stein, K. A. Bennett, F. Rivera-Hernández, V. Z. Sun, K. S. Edgett, D. M. Rubin, C. House, J. Van Beek, A lacustrine paleoenvironment recorded at Vera RubinRidge, Gale crater: Overview of the sedimentology and stratigraphy observed by the Mars Science Laboratory Curiosity Rover. *J. Geophys. Res. Planets* **125**, e2019JE006307 (2020).

15. J. P. Grotzinger, R. E. Arvidson, J. F. Bell III, W. Calvin, B. C. Clark, D. A. Fike, M. Golombek, R. Greeley, A. Haldemann, K. E. Herkenhoff, B. L. Jolliff, A. H. Knoll, M. Malin, S. M. McLennan, T. Parker, L. Soderblom, J. N. Sohl-Dickstein, S. W. Squyres, N. J. Tosca, W. A. Watters, Stratigraphy and sedimentology of a dry to wet eolian depositional system, Burns formation, Meridiani Planum, Mars. *Earth Planet. Sci. Lett.* **240**, 11–72 (2005).

16. J. P. Grotzinger, D. Y. Sumner, L. C. Kah, K. Stack, S. Gupta, L. Edgar, D. Rubin, K. Lewis, J. Schieber, N. Mangold, R. Milliken, P. G. Conrad, D. D. Marais, J. Farmer, K. Siebach, F. Calef, J. H. III, S. M. M. Lennan, D. Ming, D. Vaniman, J. Crisp, A. Vasavada, K. S. Edgett, M. Malin, D. Blake, R. Gellert, P. Mahaffy, R. C. Wiens, S. Maurice, J. A. Grant, S. Wilson, R. C. Anderson, L. Beegle, R. Arvidson, B. Hallet, R. S. Sletten, M. Rice, J. Bell, J. G. III, B. Ehlmann, R. B. Anderson, T. F. Bristow, W. E. Dietrich, G. Dromart, J. Eigenbrode, A. Fraeman, C. Hardgrove, K. Herkenhoff, L. Jandura, G. Kocurek, S. Lee, L. A. Leshin, R. Leveille, D. Limonadi, J. Maki, S. M. Closkey, M. Meyer, M. Minitti, H. Newsom, D. Oehler, A. Okon, M. Palucis, T. Parker, S. Rowland, M. Schmidt, S. Squyres, A. Steele, E. Stolper, R. Summons, A. Treiman, R. Williams, A. Yingst, MSL Science Team, O. Kemppinen, N. Bridges, J. R. Johnson, D. Cremers, J. Godber, M. Wadhwa, D. Wellington, I. M. Ewan, C. Newman, M. Richardson, A. Charpentier, L. Peret, P. King, J. Blank, G. Weigle, S. Li, K. Robertson, V. Sun, M. Baker, C. Edwards, K. Farley, H. Miller, M. Newcombe, C. Pilorget, C. Brunet, V. Hipkin, R. Léveillé, G. Marchand, P. S. Sánchez, L. Favot, G. Cody, L. Flückiger, D. Lees, A. Nefian, M. Martin, M. Gailhanou, F. Westall, G. Israël, C. Agard, J. Baroukh, C. Donny, A. Gaboriaud, P. Guillemot, V. Lafaille, E. Lorigny, A. Paillet, R. Pérez, M. Saccoccio, C. Yana, C. Armiens-Aparicio, J. C. Rodríguez, I. C. Blázquez, F. G. Gómez, J. Gómez-Elvira, S. Hettrich, A. L. Malvitte, M. M. Jiménez, J. Martínez-Frías, J. Martín-Soler, F. J. Martín-Torres, A. M. Jurado, L. Mora-Sotomayor, G. M. Caro, S. N. López, V. Peinado-González, J. Pla-García, J. A. R. Manfredi, J. J. Romeral-Planelló, S. A. S. Fuentes, E. S. Martinez, J. T. Redondo, R. Urqui-O'Callaghan, M.-P. Z. Mier, S. Chipera, J.-L. Lacour, P. Mauchien, J.-B. Sirven, H. Manning, A. Fairén, A. Hayes, J. Joseph, R. Sullivan, P. Thomas, A. Dupont, A. Lundberg, N. Melikechi, A. Mezzacappa, J. De Marines, D. Grinspoon, G. Reitz, B. Prats, E. Atlaskin, M. Genzer, A.-M. Harri, H. Haukka, H. Kahanpää, J. Kauhanen, M. Paton, J. Polkko, W. Schmidt, T. Siili, C. Fabre, J. Wray, M. B. Wilhelm, F. Poitrasson, K. Patel, S. Gorevan, S. Indyk, G. Paulsen, D. Bish, B. Gondet, Y. Langevin, C. Geffroy, D. Baratoux, G. Berger, A. Cros, c. d'Uston, O. Forni, O. Gasnault, J. Lasue, Q.-M. Lee, P.-Y. Meslin, E. Pallier, Y. Parot, P. Pinet, S. Schröder, M. Toplis, É. Lewin, W. Brunner, E. Heydari, C. Achilles, B. Sutter, M. Cabane, D. Coscia, C. Szopa, F. Robert, V. Sautter, S. L. Mouélic, M. Nachon, A. Buch, F. Stalport, P. Coll, P. François, F. Raulin, S. Teinturier, J. Cameron, S. Clegg, A. Cousin, D. De Lapp, R. Dingler, R. S. Jackson, S. Johnstone, N. Lanza, C. Little, T. Nelson, R. B. Williams, A. Jones, L. Kirkland, B. Baker, B. Cantor, M. Caplinger, S. Davis, B. Duston, D. Fay, D. Harker, P. Herrera, E. Jensen, M. R. Kennedy, G. Krezoski, D. Krysak, L. Lipkaman, E. M. Cartney, S. M. Nair, B. Nixon, L. Posiolova, M. Ravine, A. Salamon, L. Saper, K. Stoiber, K. Supulver, J. Van Beek, T. Van Beek, R. Zimdar, K. L. French, K. Iagnemma, K. Miller, F. Goesmann, W. Goetz, S. Hviid, M. Johnson, M. Lefavor, E. Lyness, E. Breves, M. D. Dyar, C. Fassett, L. Edwards, R. Haberle, T. Hoehler, J. Hollingsworth, M. Kahre, L. Keely, C. M. Kay, L. Bleacher, W. Brinckerhoff, D. Choi, J. P. Dworkin, M. Floyd, C. Freissinet, J. Garvin, D. Glavin, D. Harpold, D. K. Martin, A. M. Adam, A. Pavlov, E. Raaen, M. D. Smith, J. Stern, F. Tan, M. Trainer, A. Posner, M. Voytek, A. Aubrey, A. Behar, D. Blaney, D. Brinza, L. Christensen, L. De Flores, J. Feldman, S. Feldman, G. Flesch, I. Jun, D. Keymeulen, M. Mischna, J. M. Morookian, B. Pavri, M. Schoppers, A. Sengstacken, J. J. Simmonds, N. Spanovich, M. de la Torre Juarez, C. R. Webster, A. Yen, P. D. Archer, F. Cucinotta, J. H. Jones, R. V. Morris, P. Niles, E. Rampe, T. Nolan, M. Fisk, L. Radziemski, B. Barraclough, S. Bender, D. Berman, E. N. Dobrea, R. Tokar, T. Cleghorn, W. Huntress, G. Manhès, J. Hudgins, T. Olson, N. Stewart, P. Sarrazin, E. Vicenzi, M. Bullock, B. Ehresmann, V. Hamilton, D. Hassler, J. Peterson, S. Rafkin, C. Zeitlin, F. Fedosov, D. Golovin, N. Karpushkina, A. Kozyrev, M. Litvak, A. Malakhov, I. Mitrofanov, M. Mokrousov, S. Nikiforov, V. Prokhorov, A. Sanin, V. Tretyakov, A. Varenikov, A. Vostrukhin, R. Kuzmin, B. Clark, M. Wolff, O. Botta, D. Drake, K. Bean, M. Lemmon, S. P. Schwenzer, E. M. Lee, R. Sucharski, M. Á. de Pablo Hernández, J. J. B. Ávalos, M. Ramos, M.-H. Kim, C. Malespin, I. Plante, J.-P. Muller, R. Navarro-González, R. Ewing, W. Boynton, R. Downs, M. Fitzgibbon, K. Harshman, S. Morrison, O. Kortmann, A. Williams, G. Lugmair, M. A. Wilson, D. Jakosky, K. Balic-Zunic, J. Frydenvang, J. K. Jensen, K. Kinch, A. Koefoed, M. B. Madsen, S. L. S. Stipp, N. Boyd, J. L. Campbell, G. Perrett, I. Pradler, S. Van Bommel, S. Jacob, T. Owen, H. Savijärvi, E. Boehm, S. Böttcher, S. Burmeister, J. Guo, J. Köhler,

C. M. García, R. Mueller-Mellin, R. Wimmer-Schweingruber, J. C. Bridges, T. M. Connochie, M. Benna, H. Franz, H. Bower, A. Brunner, H. Blau, T. Boucher, M. Carmosino, S. Atreya, H. Elliott, D. Halleaux, N. Rennó, M. Wong, R. Pepin, B. Elliott, J. Spray, L. Thompson, S. Gordon, A. Ollila, J. Williams, P. Vasconcelos, J. Bentz, K. Nealson, R. Popa, J. Moersch, C. Tate, M. Day, R. Francis, E. M. Cullough, E. Cloutis, I. L. ten Kate, D. Scholes, S. Slavney, T. Stein, J. Ward, J. Berger, J. E. Moores, A habitable fluvio-lacustrine environment at Yellowknife Bay, Gale Crater, Mars. *Science* **343**, 1242777 (2014).

17. K. M. Stack, J. P. Grotzinger, M. P. Lamb, S. Gupta, D. M. Rubin, L. C. Kah, L. A. Edgar, D. M. Fey, J. A. Hurowitz, M. M. Bride, F. Rivera-Hernández, D. Y. Sumner, J. K. Van Beek, R. M. E. Williams, R. A. Yingst, Evidence for plunging river plume deposits in the Pahrump Hills member of the Murray formation, Gale crater, Mars. *Sedimentology* **66**, 1768–1802 (2019).

18. R. M. E. Williams, J. P. Grotzinger, W. E. Dietrich, S. Gupta, D. Y. Sumner, R. C. Wiens, N. Mangold, M. C. Malin, K. S. Edgett, S. Maurice, O. Forni, O. Gasnault, A. Ollila, H. E. Newsom, G. Dromart, M. C. Palucis, R. A. Yingst, R. B. Anderson, K. E. Herkenhoff, S. Le Mouélic, W. Goetz, M. B. Madsen, A. Koefoed, J. K. Jensen, J. C. Bridges, S. P. Schwenzer, K. W. Lewis, K. M. Stack, D. Rubin, L. C. Kah, J. F. Bell, J. D. F. III, R. Sullivan, T. Van Beek, D. L. Blaney, O. Pariser, R. G. Deen, MSL Science Team, O. Kemppinen, N. Bridges, J. R. Johnson, M. Minitti, D. Cremers, L. Edgar, M. Godber, M. Wadhwa, D. Wellington, I. M. Ewan, C. Newman, M. Richardson, A. Charpentier, L. Peret, P. King, J. Blank, G. Weigle, M. Schmidt, S. Li, R. Milliken, K. Robertson, V. Sun, M. Baker, C. Edwards, B. Ehlmann, K. Farley, J. Griffes, H. Miller, M. Newcombe, C. Pilorget, M. Rice, K. Siebach, E. Stolper, C. Brunet, V. Hipkin, R. Léveillé, G. Marchand, P. S. Sánchez, L. Favot, G. Cody, A. Steele, D. Flückiger, D. Lees, A. Nefian, M. Martin, M. Gailhanou, F. Westall, G. Israël, C. Agard, J. Baroukh, C. Donny, A. Gaboriaud, P. Guillemot, V. Lafaille, E. Lorigny, A. Paillet, R. Pérez, M. Saccoccio, C. Yana, C. A. Aparicio, J. C. Rodríguez, I. C. Blázquez, F. G. Gómez, J. G. Elvira, S. Hettrich, A. L. Malvitte, M. M. Jiménez, J. M. Frías, J. M. Soler, F. J. M. Torres, A. M. Jurado, L. M. Sotomayor, G. M. Caro, S. N. López, V. P. González, J. P. García, J. A. Rodriguez Manfredi, J. J. Romeral Planelló, S. A. Sans Fuentes, E. S. Martinez, J. T. Redondo, R. U. O'Callaghan, M.-P. Zorzano Mier, S. Chipera, J.-L. Lacour, P. Mauchien, J.-B. Sirven, H. Manning, A. Fairén, A. Hayes, J. Joseph, S. Squyres, P. Thomas, A. Dupont, A. Lundberg, N. Melikechi, A. Mezzacappa, J. De Marines, D. Grinspoon, G. Reitz, B. Prats, E. Atlaskin, M. Genzer, A.-M. Harri, H. Haukka, H. Kahanpää, J. Kauhanen, M. Paton, J. Polkko, W. Schmidt, T. Siili, C. Fabre, J. Wray, M. B. Wilhelm, F. Poitrasson, K. Patel, S. Gorevan, S. Indyk, G. Paulsen, D. Bish, J. Schieber, B. Gondet, Y. Langevin, C. Geffroy, D. Baratoux, G. Berger, A. Cros, C. D. Uston, J. Lasue, Q.-M. Lee, P.-Y. Meslin, E. Pallier, Y. Parot, P. Pinet, S. Schröder, M. Toplis, É. Lewin, W. Brunner, E. Heydari, C. Achilles, D. Oehler, B. Sutter, M. Cabane, D. Coscia, C. Szopa, F. Robert, V. Sautter, M. Nachon, A. Buch, F. Stalport, P. Coll, P. François, F. Raulin, S. Teinturier, J. Cameron, S. Clegg, A. Cousin, D. De Lapp, R. Dingler, R. S. Jackson, S. Johnstone, N. Lanza, C. Little, T. Nelson, R. B. Williams, A. Jones, L. Kirkland, A. Treiman, B. Baker, B. Cantor, M. Caplinger, S. Davis, B. Duston, D. Fay, C. Hardgrove, D. Harker, P. Herrera, E. Jensen, M. R. Kennedy, G. Krezoski, D. Krysak, L. Lipkaman, E. M. Cartney, S. M. Nair, B. Nixon, L. Posiolova, M. Ravine, A. Salamon, L. Saper, K. Stoiber, K. Supulver, J. Van Beek, R. Zimdar, K. L. French, K. Iagnemma, K. Miller, R. Summons, F. Goesmann, W. Goetz, S. Hviid, M. Johnson, M. Lefavor, E. Lyness, E. Breves, M. D. Dyar, C. Fassett, D. F. Blake, T. Bristow, D. D. Marais, L. Edwards, R. Haberle, T. Hoehler, J. Hollingsworth, M. Kahre, L. Keely, C. M. Kay, L. Bleacher, W. Brinckerhoff, D. Choi, P. Conrad, J. P. Dworkin, J. Eigenbrode, M. Floyd, C. Freissinet, J. Garvin, D. Glavin, D. Harpold, P. Mahaffy, D. K. Martin, A. M. Adam, A. Pavlov, E. Raaen, M. D. Smith, J. Stern, F. Tan, M. Trainer, M. Meyer, A. Posner, M. Voytek, R. C. Anderson, A. Aubrey, L. W. Beegle, A. Behar, D. Brinza, F. Calef, L. Christensen, J. A. Crisp, L. De Flores, J. Feldman, S. Feldman, G. Flesch, J. Hurowitz, I. Jun, D. Keymeulen, J. Maki, M. Mischna, J. M. Morookian, T. Parker, B. Pavri, M. Schoppers, A. Sengstacken, J. J. Simmonds, N. Spanovich, M. de la Torre Juarez, A. R. Vasavada, C. R. Webster, A. Yen, P. D. Archer, F. Cucinotta, J. H. Jones, D. Ming, R. V. Morris, P. Niles, E. Rampe, T. Nolan, M. Fisk, L. Radziemski, B. Barraclough, S. Bender, D. Berman, E. N. Dobrea, R. Tokar, D. Vaniman, L. Leshin, T. Cleghorn, W. Huntress, G. Manhès, J. Hudgins, T. Olson, N. Stewart, P. Sarrazin, J. Grant, E. Vicenzi, S. A. Wilson, M. Bullock, B. Ehresmann, V. Hamilton, D. Hassler, J. Peterson, S. Rafkin, C. Zeitlin, F. Fedosov, D. Golovin, N. Karpushkina, A. Kozyrev, M. Litvak, A. Malakhov, I. Mitrofanov, M. Mokrousov, S. Nikiforov, V. Prokhorov, A. Sanin, V. Tretyakov, A. Varenikov, A. Vostrukhin, R. Kuzmin, B. Clark, M. Wolff, S. M. Lennan, O. Botta, D. Drake, K. Bean, M. Lemmon, E. M. Lee, R. Sucharski, M. Á. de Pablo Hernández, J. J. B. Ávalos, M. Ramos, M.-H. Kim, C. Malespin, I. Plante, J.-P. Muller, R. Navarro-González, R. Ewing, W. Boynton, R. Downs, M. Fitzgibbon, K. Harshman, S. Morrison, O. Kortmann, A. Williams, G. Lugmair, M. A. Wilson, B. Jakosky, T. B. Zunic, J. Frydenvang, K. Kinch, S. L. S. Stipp, N. Boyd, J. L. Campbell, R. Gellert, G. Perrett, I. Pradler, S. Van Bommel, S. Jacob, T. Owen, S. Rowland, H. Savijärvi, E. Boehm, S. Böttcher, S. Burmeister, J. Guo, J. Köhler, C. M. García, R. M. Mellin, R. W. Schweingruber, T. M. Connochie, M. Benna, H. Franz, H. Bower, A. Brunner, H. Blau, T. Boucher, M. Carmosino, S. Atreya, H. Elliott, D. Halleaux, N. Rennó, M. Wong, R. Pepin, B. Elliott, J. Spray, L. Thompson, S. Gordon, J. Williams, P. Vasconcelos, J. Bentz, K. Nealson, R. Popa, J. Moersch, C. Tate, M. Day, G. Kocurek, B. Hallet, R. Sletten, R. Francis, E. M. Cullough, E. Cloutis, I. L. ten Kate,

R. Arvidson, A. Fraeman, D. Scholes, S. Slavney, T. Stein, J. Ward, J. Berger, J. E. Moores, Martian fluvial conglomerates at Gale crater. *Science* **340**, 1068–1072 (2013).

19. L. Edgar, J. Grotzinger, C. M. Fedo, M. Meyer, W. Rapin, W. E. Dietrich, A. B. Bryk, S. Gupta, A. L. Roberts, S. G. Banham, J. Reahl, Wet to dry depositional environments recorded in the clay-sulfate transition region in Gale crater, Mars: Overview and stratigraphic context for Curiosity's exploration campaign, in *55th Lunar and Planetary Science Conference* (Lunar and Planetary Institute, 2024), p. 1016.

20. S. W. Squyres, J. F. Kasting, Early Mars: How warm and how wet? *Science* **265**, 744–749 (1994).

21. C. P. McKay, D. T. Andersen, W. H. Pollard, J. L. Heldmann, P. T. Doran, C. H. Fritsen, J. C. Priscu, 9 Polar lakes, streams, and springs as analogs for the hydrological cycle on Mars, in *Water on Mars and Life* (Springer, 2005), pp. 219–233.

22. E. S. Kite, Geologic constraints on early Mars climate. *Space Sci. Rev.* **215**, 10 (2019).

23. L. Le Deit, E. Hauber, F. Fueten, M. Pondrelli, A. P. Rossi, R. Jaumann, Sequence of infilling events in Gale Crater, Mars: Results from morphology, stratigraphy, and mineralogy. *J. Geophys. Res. Planets* **118**, 2439–2473 (2013).

24. J. P. Grotzinger, S. Gupta, M. C. Malin, D. M. Rubin, J. Schieber, K. Siebach, D. Y. Sumner, K. M. Stack, A. R. Vasavada, R. E. Arvidson, F. Calef III, L. Edgar, W. F. Fischer, J. A. Grant, J. Griffes, L. C. Kah, M. P. Lamb, K. W. Lewis, N. Mangold, M. E. Minitti, M. Palucis, M. Rice, R. M. E. Williams, R. A. Yingst, D. Blake, D. Blaney, P. Conrad, J. Crisp, W. E. Dietrich, G. Dromart, K. S. Edgett, R. C. Ewing, R. Gellert, J. A. Hurowitz, G. Kocurek, P. Mahaffy, M. J. McBride, S. M. McLennan, M. Mischna, D. Ming, R. Milliken, H. Newsom, D. Oehler, T. J. Parker, D. Vaniman, R. C. Wiens, S. A. Wilson, Deposition, exhumation, and paleoclimate of an ancient lake deposit, Gale crater, Mars. *Science* **350**, aac7575 (2015).

25. C. M. Fedo, A. B. Bryk, L. A. Edgar, K. A. Bennett, V. K. Fox, W. E. Dietrich, S. G. Banham, S. Gupta, K. M. Stack, R. M. E. Williams, J. P. Grotzinger, N. T. Stein, D. M. Rubin, G. Caravaca, R. E. Arvidson, M. N. Hughes, A. A. Fraeman, A. R. Vasavada, J. Schieber, B. Sutter, Geology and stratigraphic correlation of the Murray and Carolyn Shoemaker formations across the Glen Torridon region, Gale crater, Mars. *J. Geophys. Res. Planets* **127**, e2022JE007408 (2022).

26. N. T. Stein, D. P. Quinn, J. P. Grotzinger, C. Fedo, B. L. Ehlmann, K. M. Stack, L. A. Edgar, A. A. Fraeman, R. Deen, Regional structural orientation of the Mount Sharp group revealed by in situ dip measurements and stratigraphic correlations on the Vera Rubin ridge. *J. Geophys. Res. Planets* **125**, e2019JE006298 (2020).

27. S. Gwizd, C. Fedo, J. Grotzinger, S. Banham, F. Rivera-Hernández, K. M. Stack, K. Siebach, M. Thorpe, L. Thompson, C. O'Connell-Cooper, N. Stein, L. Edgar, S. Gupta, D. Rubin, D. Sumner, A. R. Vasavada, Sedimentological and geochemical perspectives on a marginal lake environment recorded in the Hartmann's Valley and Karasburg members of the Murray formation, Gale crater, Mars. *J. Geophys. Res. Planets* **127**, e2022JE007280 (2022).

28. S. Gwizd, C. Fedo, J. Grotzinger, S. Banham, F. Rivera-Hernández, S. Gupta, K. M. Stack, L. A. Edgar, A. R. Vasavada, J. Davis, L. C. Kah, Evolution of a lake margin recorded in the sutton island member of the Murray Formation, Gale Crater, Mars. *J. Geophys. Res. Planets* **129**, e2023JE007919 (2024).

29. J. Schieber, K. M. Bohacs, M. Coleman, D. Bish, M. H. Reed, L. Thompson, W. Rapin, Z. Yawar, Mars is a mirror—Understanding the Pahrump Hills mudstones from a perspective of Earth analogues. *Sedimentology* **69**, 2371–2435 (2022).

30. G. Caravaca, N. Mangold, E. Dehouck, J. Schieber, L. Zaugg, A. B. Bryk, C. M. Fedo, S. L. Mouélic, L. L. Deit, S. G. Banham, S. Gupta, A. Cousin, W. Rapin, O. Gasnault, F. Rivera-Hernández, R. C. Wiens, N. L. Lanza, From lake to river: Documenting an environmental transition across the Jura/Knockfarril Hill members boundary in the Glen Torridon region of Gale crater (Mars). *J. Geophys. Res. Planets* **127**, e2021JE007093 (2022).

31. B. T. Cardenas, J. P. Grotzinger, M. P. Lamb, K. W. Lewis, C. M. Fedo, A. B. Bryk, W. E. Dietrich, N. Stein, M. Turner, G. Caravaca, Barform deposits of the Carolyn Shoemaker formation, Gale crater, Mars. *J. Sediment. Res.* **92**, 1071–1092 (2022).

32. S. Gupta, L. Edgar, R. A. Yingst, A. B. Bryk, G. Caravaca, W. Dietrich, J. Grotzinger, D. Rubin, W. Rapin, S. Banham, A. Roberts, S. Le Mouélic, R. Williams, J. Schieber, N. Mangold, T. Kubacki, O. Gasnault, R. Wiens, A. Fraeman, A. Vasavada, Episodic aqueous conditions punctuated dominantly aeolian deposition within the layered sulphate-bearing unit, Gale crater (Mars), in *Europlanet Science Congress* (Europlanet Society, 2022), pp. EPSC2022–963.

33. R. E. Milliken, J. P. Grotzinger, B. J. Thomson, Paleoclimate of Mars as captured by the stratigraphic record in Gale Crater. *Geophys. Res. Lett.* **37**, L04201 (2010).

34. C. M. Weitz, K. W. Lewis, J. L. Bishop, B. J. Thomson, R. E. Arvidson, J. A. Grant, K. D. Seelos, I. Ettenborough, Orbital observations of a marker horizon at Gale crater. *J. Geophys. Res. Planets* **127**, e2022JE007211 (2022).

35. P. L. Wiberg, C. K. Harris, Ripple geometry in wave-dominated environments. *J. Geophys. Res. Oceans* **99**, 775–789 (1994).

36. K. S. Edgett, R. A. Yingst, M. A. Ravine, M. A. Caplinger, J. N. Maki, F. T. Ghaemi, J. A. Schaffner, J. F. Bell III, L. J. Edwards, K. E. Herkenhoff, E. Heydari, L. C. Kah, M. T. Lemmon, M. E. Minitti, T. S. Olson, T. J. Parker, S. K. Rowland, J. Schieber, R. J. Sullivan, D. Y. Sumner, P. C. Thomas, E. H. Jensen, J. J. Simmonds, A. J. Sengstacken, R. G. Willson,

W. Goetz, Curiosity's Mars hand lens imager (MAHLI) investigation. *Space Sci. Rev.* **170**, 259–317 (2012).

37. J. F. M. De Raaf, J. R. Boersma, S. Van Gelder, Wave-generated structures and sequences from a shallow marine succession, Lower Carboniferous, County Cork, Ireland. *Sedimentology* **24**, 451–483 (1977).

38. M. G. A. Lapotre, M. P. Lamb, B. McElroy, What sets the size of current ripples? *Geology* **45**, 243–246 (2017).

39. W. F. Tanner, Ripple mark indices and their uses. *Sedimentology* **9**, 89–104 (1967).

40. S. Dumas, R. W. C. Arnott, J. B. Southard, Experiments on oscillatory-flow and combined-flow bed forms: Implications for interpreting parts of the shallow-marine sedimentary record. *J. Sediment. Res.* **75**, 501–513 (2005).

41. M. E. Brookfield, S. Silvestro, Eolian systems, in *Facies Models 4* (Geological Association of Canada, 2010), pp. 139–166.

42. G. Kocurek, J. Nielson, Conditions favourable for the formation of warm-climate aeolian sand sheets. *Sedimentology* **33**, 795–816 (1986).

43. J. Schwan, The structure and genesis of Weichselian to early hologene aeolian sand sheets in western Europe. *Sediment. Geol.* **55**, 197–232 (1988).

44. G. M. Ashley, J. B. Southard, J. C. Boothroyd, Deposition of climbing-ripple beds: A flume simulation. *Sedimentology* **29**, 67–79 (1982).

45. J. Grotzinger, J. Bell III, K. Herkenhoff, J. Johnson, A. Knoll, E. McCartney, S. McLennan, J. Metz, J. Moore, S. Squyres, R. Sullivan, O. Ahronson, R. Arvidson, B. Joliff, M. Golombek, K. Lewis, T. Parker, J. Soderblom, Sedimentary textures formed by aqueous processes, Erebus crater, Meridiani Planum, Mars. *Geology* **34**, 1085–1088 (2006).

46. D. M. Rubin, J. C. Schmidt, J. N. Moore, Origin, structure, and evolution of a reattachment bar, Colorado River, Grand Canyon, Arizona. *J. Sediment. Res.* **60**, 982–991 (1990).

47. J. R. Dingler, H. E. Clifton, Tidal-cycle changes in oscillation ripples on the inner part of an estuarine sand flat. *Mar. Geol.* **60**, 219–233 (1984).

48. G. M. Martínez, C. N. Newman, A. De Vicente-Retortillo, E. Fischer, N. O. Renno, M. I. Richardson, A. G. Fairén, M. Genzer, S. D. Guzewich, R. M. Haberle, A.-M. Harri, O. Kemppinen, M. T. Lemmon, M. D. Smith, M. de la Torre-Juárez, A. R. Vasavada, The modern near-surface Martian climate: A review of in-situ meteorological data from Viking to Curiosity. *Space Sci. Rev.* **212**, 295–338 (2017).

49. S. G. Banham, S. Gupta, D. M. Rubin, K. S. Edgett, R. Barnes, J. Van Beek, J. A. Watkins, L. A. Edgar, C. M. Fedo, R. M. Williams, K. M. Stack, J. P. Grotzinger, K. Lewis, R. C. Ewing, M. Day, A. R. Vasavada, A rock record of complex aeolian bedforms in a Hesperian desert landscape: The Stimson formation as exposed in the Murray buttes, Gale crater, Mars. *J. Geophys. Res. Planets* **126**, e2020JE006554 (2021).

50. T. F. Bristow, J. P. Grotzinger, E. B. Rampe, J. Cuadros, S. J. Chipera, G. W. Downs, C. M. Fedo, J. Frydenvang, A. C. McAdam, R. V. Morris, C. N. Achilles, D. F. Blake, N. Castle, P. Craig, D. J. D. Marais, R. T. Downs, R. M. Hazen, D. W. Ming, S. M. Morrison, M. T. Thorpe, A. H. Treiman, V. Tu, D. T. Vaniman, A. S. Yen, R. Gellert, P. R. Mahaffy, R. C. Wiens, A. B. Bryk, K. A. Bennett, V. K. Fox, R. E. Millken, A. A. Fraeman, A. R. Vasavada, Brine-driven destruction of clay minerals in Gale crater, Mars. *Science* **373**, 198–204 (2021).

51. L. A. Edgar, J. P. Grotzinger, A. G. Hayes, D. M. Rubin, S. W. Squyres, J. F. Bell, K. E. Herkenhoff, Stratigraphic architecture of bedrock reference section, Victoria Crater, Meridiani Planum, Mars, in *Sedimentary Geology of Mars* (SEPM Special Publication No. 102, 2012), pp. 195–209.

52. K. W. Lewis, O. Aharonson, J. P. Grotzinger, S. W. Squyres, J. F. Bell III, L. S. Crumpler, M. E. Schmidt, Structure and stratigraphy of home plate from the spirit mars exploration rover. *J. Geophys. Res. Planets* **113**, E12S36 (2008).

53. J. M. Metz, J. P. Grotzinger, D. Mohrig, R. Milliken, B. Prather, C. Pirmez, A. S. McEwen, C. M. Weitz, Sublacustrine depositional fans in southwest Melas Chasma. *J. Geophys. Res. Planets* **114**, E10002 (2009).

54. P. M. Myrow, M. P. Lamb, R. C. Ewing, Rapid sea level rise in the aftermath of a Neoproterozoic snowball Earth. *Science* **360**, 649–651 (2018).

55. Coastal Engineering Research Center, Shore Protection Manual (US Army Corps of Engineers, 1984).

56. M. P. Lamb, W. W. Fischer, T. D. Raub, J. T. Perron, P. M. Myrow, Origin of giant wave ripples in snowball Earth cap carbonate. *Geology* **40**, 827–830 (2012).

57. Z.-J. You, B. Yin, A unified criterion for initiation of sediment motion and inception of sheet flow under water waves. *Sedimentology* **53**, 1181–1190 (2006).

58. M. C. Malin, M. A. Ravine, M. A. Caplinger, F. T. Ghaemi, J. A. Schaffner, J. N. Maki, J. F. Bell III, J. F. Cameron, W. E. Dietrich, K. S. Edgett, L. J. Edwards, J. B. Garvin, B. Hallet, K. E. Herkenhoff, E. Heydari, L. C. Kah, M. T. Lemmon, M. E. Minitti, T. S. Olson, T. J. Parker, S. K. Rowland, J. Schieber, R. Sletten, R. J. Sullivan, D. Y. Sumner, R. A. Yingst, B. M. Duston, S. M. Nair, E. H. Jensen, The Mars Science Laboratory (MSL) mast cameras and descent imager: Investigation and instrument descriptions. *Earth Space Sci.* **4**, 506–539 (2017).

59. S. Le Mouélic, O. Gasnault, K. E. Herkenhoff, N. T. Bridges, Y. Langevin, N. Mangold, S. Maurice, R. C. Wiens, P. Pinet, H. E. Newsom, R. G. Deen, J. F. Bell III, J. R. Johnson, W. Rapin, B. Barraclough, D. L. Blaney, J. Maki, M. C. Malin, R. Perez, M. Saccoccio, The ChemCam Remote Micro-Imager at Gale crater: Review of the first year of operations on Mars. *Icarus* **249**, 93–107 (2015).

60. J. Maki, D. Thiessen, A. Pourangi, P. Kobzeff, T. Litwin, L. Scherr, S. Elliott, A. Dingizian, M. Maimone, The Mars Science Laboratory engineering cameras. *Space Sci. Rev.* **170**, 77–93 (2012).

61. F. J. Calef III, T. Parker, MSL Gale Merged Orthophoto Mosaic, PDS Annex, U.S. Geological Survey (2016); https://astrogeology.usgs.gov/search/map/mars_msl_gale_merged_orthophoto_mosaic_25cm.

62. F. J. Calef, T. Soliman, H. E. Abarca, S. P. Abercrombie, M. W. Powell, Multi-mission geographic information system: An open source solution for planetary science operation, in *4th Planetary Data Workshop* (Lunar and Planetary Institute, 2019), p. 7071.

63. A. S. McEwen, E. M. Eliason, J. W. Bergstrom, N. T. Bridges, C. J. Hansen, W. A. Delamere, J. A. Grant, V. C. Gulick, K. E. Herkenhoff, L. Keszthelyi, R. L. Kirk, M. T. Mellon, S. W. Squyres, N. Thomas, C. M. Weitz, Mars reconnaissance orbiter's high resolution imaging science experiment (HiRISE). *J. Geophys. Res. Planets* **112**, E05S02 (2007).

64. H. Tennekes, J. L. Lumley, *A First Course in Turbulence* (MIT Press, 1972).

65. P. D. Komar, *Beach Processes and Sedimentation* (Prentice Hall, 1998).

66. F. Pedocchi, M. H. García, Ripple morphology under oscillatory flow: 2. Experiments. *J. Geophys. Res. Oceans* **114**, C12015 (2009).

67. L. Braat, M. Z. M. Bückner, E. Sefton-Nash, M. P. Lamb, Gravity-driven differences in fluvial sediment transport fluxes on Mars and Earth. *J. Geophys. Res. Planets* **129**, e2023JE007788 (2024).

68. J. B. Southard, L. A. Boguchwal, Bed configurations in steady unidirectional water flows: 3. Effects of temperature and gravity. *J. Sediment. Petrol.* **60**, 680–686 (1990).

69. M. H. García, Sediment transport and morphodynamics, in *Sedimentation Engineering; Processes, Measurements, Modeling, and Practice* (American Society of Civil Engineers, 2008), pp. 21–163.

70. M. P. Lamb, J. Grotzinger, J. B. Southard, N. Tosca, Were ripples on Mars formed by flowing brines?, in *Sedimentary Geology on Mars* (SEPM Special Publication No. 102, 2012), pp. 139–150.

71. R. W. C. Arnott, J. B. Southard, Exploratory flow-duct experiments on combined-flow bed configurations, and some implications for interpreting storm-event stratification. *J. Sediment. Petrol.* **60**, 211–219 (1990).

72. J. H. Nienhuis, J. T. Perron, J. C. T. Kao, P. M. Myrow, Wavelength selection and symmetry breaking in orbital wave ripples. *J. Geophys. Res. Earth* **119**, 2239–2257 (2014).

73. J. C. Harms, J. B. Southard, R. G. Walker, Structures and sequences in clastic rocks: Society of Economic Paleontologists and Mineralogists Short Course Notes No. 9 (1982), pp. 2–55.

Science Advances

Wave ripples formed in ancient, ice-free lakes in Gale crater, Mars

Claire A. Mondro, Christopher M. Fedo, John P. Grotzinger, Michael P. Lamb, Sanjeev Gupta, William E. Dietrich, Steven Banham, Catherine M. Weitz, Patrick Gasda, Lauren A. Edgar, David Rubin, Alexander B. Bryk, Edwin S. Kite, Gwénaël Caravaca, Juergen Schieber, and Ashwin R. Vasavada

View the article online
https://www.science.org/doi/10.1126/sciadv.adr0010
Permissions
https://www.science.org/help/reprints-and-permissions

Use of this article is subject to the Terms of service